Dipolar thermocapillary motor and swimmer

Valeri Frumkin,[1] Khaled Gommed,[1] and Moran Bercovici[1,2,*]

[1]*Faculty of Mechanical Engineering, Technion - Israel Institute of Technology, Haifa 3200003, Israel*
[2]*Department of Mechanical Engineering, The University of Texas at Austin, Austin, Texas 78712, USA*

The study of thermocapillary driven flows is typically restricted to "open" systems, i.e., ones where a liquid film is bounded on one side solely by another fluid. However, a large number of natural and engineered fluidic systems are composed of solid boundaries with only small open regions exposed to the surrounding. In this work we study the flow generated by the thermocapillary effect in a liquid film overlaid by a discontinuous solid surface. If the openings in the solid are subjected to a temperature gradient, the resulting thermocapillary flow will lead to a nonuniform pressure distribution in the film, driving flow in the rest of the system. For an infinite solid surface containing circular openings, we show that the resulting pressure distribution yields dipole flows which can be superposed to create complex flow patterns, and demonstrate how a confined dipole can act as a thermocapillary motor for driving fluids in closed microfluidic circuits. For a mobile, finite-size surface, we show that an inner temperature gradient, which can be activated by simple illumination, results in the propulsion of the surface, creating a thermocapillary surface swimmer.

I. INTRODUCTION

When an interface between two immiscible fluids is subjected to a nonuniform temperature distribution, the dependence of surface tension on temperature gives rise to tangential stresses which drive fluid motion along the interface. This phenomena, termed the thermocapillary or (more generally) the Marangoni effect, is of central importance in the field of microfluidics due to the dominance of surface forces over body forces at the microscale [1]. A nonexhaustive list of applications in this field includes the manipulation and production of droplets [2,3], thermocapillary ratchet flows [4], patterning of nanoscale polymer films [5], and optical manipulation of microscale fluid flow [6]. More recent works demonstrated that laser induced thermocapillary flow can be used in order to convert light into mechanical work [7,8] or manipulate micron-sized particles at fluid-liquid interfaces [9]. Theoretical work also suggested enclosing a fluid-liquid interface within microdevices such as microchannels [10,11] and Hele-Shaw chambers [12], as means of fluid transport. However, all of the above examples make use of a continuous fluid-liquid interface, while many engineering realizations of such systems may include the interaction of free surfaces with no-slip boundaries. While a number of theoretical studies analyzed flows over superhydrophobic surfaces as a particular case of such interactions, predicting an effective slip [13,14], such effectively continuous behavior can only be obtained for periodic systems. To the best of our knowledge, thermocapillary flows over macroscale, nonperiodic solid discontinuities have not yet been addressed.

---

*Corresponding author: mberco@technion.ac.il
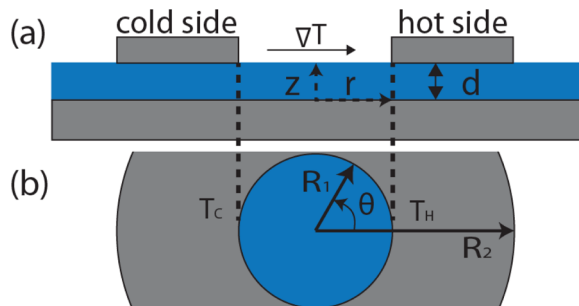
FIG. 1. Schematic of the system's geometry: (a) Side view of the suspended surface with the circular opening. A temperature gradient is induced from left to right, resulting in a gradient in surface tension in the opposite direction. (b) Top view of the annulus.

In this work, we study analytically and experimentally the case of a thin liquid film, overlaid by a solid surface containing a circular gap, exposing a limited free surface region. For the case of an infinite and stationary surface, we show that the resulting pressure distribution gives rise to dipole flow in the closed region. Such dipoles can be superposed to create more complex (but well predicted flows). For the case of a finite mobile surface, i.e., a floating annulus, we show that the same phenomenon results in propulsion of the object. Finally, we also show that such propulsion can be actuated by simple illumination, creating photoactivated surface swimmers. We here present our theoretical analysis, followed by experimental demonstration and validation.

II. PROBLEM FORMULATION

As illustrated in Fig. 1, we consider an annulus with inner radius R_1 and outer radius R_2, floating on a thin liquid film of height d, viscosity μ, and density ρ, overlaying a continuous rigid surface. A uniform temperature gradient is induced across the inner opening of the annulus, initiating thermocapillary flow there and resulting in the propulsion of the annulus with a steady state velocity V in the direction opposite to that of the temperature gradient. We assume the free surface in all regions to be nondeformable, and that the inner radius R_1 is much greater than d, giving rise to a natural small parameter for the system $\epsilon = d/R_1 \ll 1$. We model the system using the steady-state Navier-Stokes and continuity equations in a cylindrical coordinate system, whose origin coincides with the center of the circular opening moving at a constant velocity V,

$$\rho \vec{\tilde{u}} \cdot \vec{\tilde{\nabla}} \vec{\tilde{u}} = -\vec{\tilde{\nabla}} \tilde{p} + \mu \tilde{\nabla}^2 \vec{\tilde{u}}, \tag{1}$$

and the continuity equation,

$$\vec{\tilde{\nabla}} \cdot \vec{\tilde{u}} = 0, \tag{2}$$

where $\vec{\tilde{u}} = (\tilde{u}_r, \tilde{u}_\theta, \tilde{u}_z)$ is the velocity vector field, $\tilde{p}$ is the pressure, and $\vec{\tilde{\nabla}} = (\frac{\partial}{\partial \tilde{r}}, \frac{1}{\tilde{r}} \frac{\partial}{\partial \tilde{\theta}}, \frac{\partial}{\partial \tilde{z}})$.

We a assume a no-slip condition at the solid-liquid interfaces, a no-shear condition outside the annulus, and a tangential stress balance at the free surface inside the annulus, $\tilde{z} = d$, $\tilde{r} < R_1$:

$$\frac{\partial \tilde{\sigma}}{\partial \tilde{r}} = \sigma_T \frac{\partial \tilde{T}}{\partial \tilde{r}} = \mu \left(\frac{\partial \tilde{u}_z}{\partial \tilde{r}} + \frac{\partial \tilde{u}_r}{\partial \tilde{z}} \right), \tag{3a}$$

$$\frac{\partial \tilde{\sigma}}{\partial \tilde{\theta}} = \sigma_T \frac{\partial \tilde{T}}{\partial \tilde{\theta}} = \mu \left(\frac{\partial \tilde{u}_z}{\partial \tilde{\theta}} + \tilde{r} \frac{\partial \tilde{u}_\theta}{\partial \tilde{z}} \right), \tag{3b}$$

where $\sigma_T = \partial \tilde{\sigma}/\partial \tilde{T}$. We assume a linear temperature gradient across the inner opening of the annulus, given by the temperature distribution

$$\tilde{T}(\theta) = T_C + \frac{\Delta}{2}\left(1 + \frac{\tilde{r}}{R_1}\cos\tilde{\theta}\right), \quad -\pi \leqslant \tilde{\theta} \leqslant \pi, \tag{4}$$

where $\Delta = T_H - T_C$ is the maximal temperature difference across the opening. We denote all the dimensional variables with tilde, and define dimensionless variables in the following way:

$$\tilde{r} = R_1 r, \quad \tilde{\theta} = \theta, \quad \tilde{z} = dz, \quad \tilde{u}_r = U u_r, \quad \tilde{u}_\theta = U u_\theta, \quad \tilde{u}_z = \epsilon U u_z, \quad \tilde{T} = T\Delta + \bar{T}, \quad \tilde{p} = \frac{\mu U}{R_1 \epsilon^2}p, \tag{5}$$

where $\bar{T} = \frac{T_H + T_C}{2}$ is the average temperature, $\epsilon = \frac{d}{R_1} \ll 1$ is the ratio of film thickness to the inner radius of the annulus, and $U = \frac{\epsilon \sigma_T \Delta}{\mu}$ is the characteristic velocity as determined from the stress balance at the free surface, and represents the ratio between the characteristic Marangoni and viscous stresses. The dimensionless problem is then given by

$$\epsilon \mathrm{Re}\left(u_r \frac{\partial u_r}{\partial r} + \frac{u_\theta}{r}\frac{\partial u_r}{\partial \theta} + u_z \frac{\partial u_r}{\partial z} - \frac{u_\theta^2}{r}\right)$$
$$= -\frac{\partial p}{\partial r} + \epsilon^2\left[\frac{1}{r}\frac{\partial}{\partial r}\left(r\frac{\partial u_r}{\partial r}\right) - \frac{u_r}{r^2} + \frac{1}{r^2}\frac{\partial^2 u_r}{\partial \theta^2} - \frac{2}{r^2}\frac{\partial u_\theta}{\partial \theta}\right] + \frac{\partial^2 u_r}{\partial z^2}, \tag{6a}$$

$$\epsilon \mathrm{Re}\left(u_r \frac{\partial u_\theta}{\partial r} + \frac{u_\theta}{r}\frac{\partial u_\theta}{\partial \theta} + u_z \frac{\partial u_\theta}{\partial z} + \frac{u_\theta u_r}{r}\right)$$
$$= -\frac{1}{r}\frac{\partial p}{\partial \theta} + \epsilon^2\left[\frac{1}{r}\frac{\partial}{\partial r}\left(r\frac{\partial u_\theta}{\partial r}\right) - \frac{u_\theta}{r^2} + \frac{1}{r^2}\frac{\partial^2 u_\theta}{\partial \theta^2} + \frac{2}{r^2}\frac{\partial u_r}{\partial \theta}\right] + \frac{\partial^2 u_\theta}{\partial z^2}, \tag{6b}$$

$$\epsilon^2 \mathrm{Re}\left(u_r \frac{\partial u_z}{\partial r} + \frac{u_\theta}{r}\frac{\partial u_z}{\partial \theta} + u_z \frac{\partial u_z}{\partial z}\right)$$
$$= -\frac{\partial p}{\partial z} + \epsilon^3\left[\frac{1}{r}\frac{\partial}{\partial r}\left(r\frac{\partial u_z}{\partial r}\right) + \frac{1}{r^2}\frac{\partial^2 u_z}{\partial \theta^2}\right] + \epsilon\frac{\partial^2 u_z}{\partial z^2}\frac{1}{r}\frac{\partial(ru_r)}{\partial r} + \frac{1}{r}\frac{\partial u_\theta}{\partial \theta} + \frac{\partial u_z}{\partial z}, \tag{6c}$$

where $\mathrm{Re} = \frac{\rho U d}{\mu}$ is the Reynolds number. The temperature at the free surface now takes the form

$$T(\theta) = \frac{r}{2}\cos\theta, \quad -\pi \leqslant \theta \leqslant \pi, \ 0 \leqslant r \leqslant 1, \tag{7}$$

and the boundary conditions at $z = 1$ can now be written as

$$\vec{\nabla}_\| T = \frac{\partial \vec{u}}{\partial z} + \epsilon^2 \vec{\nabla}_\| u \quad \text{for } r < 1, \tag{8a}$$

$$\vec{u} = 0 \quad\quad\quad\quad \text{for } 1 < r < \delta, \tag{8b}$$

$$\frac{\partial \vec{u}}{\partial z} = 0 \quad\quad\quad\quad \text{for } r > \delta, \tag{8c}$$

where $\vec{\nabla}_\| = (\frac{\partial}{\partial r}, \frac{1}{r}\frac{\partial}{\partial \theta})$, $\delta = \frac{R_2}{R_1}$, and $\vec{u} = (u_r, u_\theta)$. Since we expect the annulus to be moving at a steady velocity V in the direction opposite to that of the temperature gradient, in a frame of reference which is moving together with the annulus, the no-slip boundary condition at the bottom of the chamber translates into

$$\text{for } z = 0, \quad \vec{u} = V\hat{x}. \tag{9}$$

III. SOLUTION OF THE GOVERNING EQUATIONS

We seek solutions in terms of asymptotic expansions

$$\vec{u} = \vec{u}_0 + \epsilon \vec{u}_1 + O(\epsilon^2), \quad u_z = u_{z0} + \epsilon u_{z1} + O(\epsilon^2), \quad p = p_0 + \epsilon p_1 + O(\epsilon^2), \tag{10}$$

which, at the leading order in ϵ, yield the equations

$$\vec{\nabla}_{\parallel} p_0 = \frac{\partial^2 \vec{u}_0}{\partial z^2}, \quad \frac{\partial p_0}{\partial z} = 0, \tag{11a}$$

$$\frac{1}{r} \frac{\partial(r u_{r0})}{\partial r} + \frac{1}{r} \frac{\partial u_{\theta 0}}{\partial \theta} + \frac{\partial u_{z0}}{\partial z} = 0, \tag{11b}$$

with the boundary conditions at $z = 1$

$$\vec{\nabla}_{\parallel} T = \frac{\partial \vec{u}_0}{\partial z} \quad \text{for } r < 1, \tag{12a}$$

$$\vec{u}_0 = 0 \qquad \text{for } 1 < r < \delta, \tag{12b}$$

$$\frac{\partial \vec{u}_0}{\partial z} = 0 \qquad \text{for } \delta < r, \tag{12c}$$

and $\vec{u}_0 = V\hat{x} = V \frac{\vec{\nabla}_{\parallel} T}{|\vec{\nabla}_{\parallel} T|}$ at $z = 0$. Since under the chosen scaling $|\vec{\nabla}_{\parallel} T| = 2$,

$$\text{for } z = 0, \quad \vec{u}_0 = 2V \vec{\nabla}_{\parallel} T. \tag{13}$$

The solution for the velocity at the leading order in ϵ is given by

$$\vec{u}_0 = \begin{cases} \vec{\nabla}_{\parallel} p_0 \left(\frac{z^2}{2} - z \right) + \vec{\nabla}_{\parallel} T (z + 2V), & 0 \leqslant r < 1, \\ \frac{1}{2} \vec{\nabla}_{\parallel} p_0 (z^2 - z) + 2V \vec{\nabla}_{\parallel} T (1 - z), & 1 < r \leqslant \delta, \\ \vec{\nabla}_{\parallel} p_0 \left(\frac{z^2}{2} - z \right) + 2V \vec{\nabla}_{\parallel} T, & \delta \leqslant r, \end{cases} \tag{14}$$

which, while accounting for the boundary conditions, can be integrated to obtain an average in-plane velocity

$$\langle \vec{u}_0 \rangle = \int_0^1 \vec{u}_0 \, dz = \begin{cases} -\frac{1}{3} \vec{\nabla}_{\parallel} p_0 + \vec{\nabla}_{\parallel} T \left(\frac{1}{2} + 2V \right), & 0 \leqslant r < 1, \\ -\frac{1}{12} \vec{\nabla}_{\parallel} p_0 + V \vec{\nabla}_{\parallel} T, & 1 < r < \delta, \\ -\frac{1}{3} \vec{\nabla}_{\parallel} p_0 + 2V \vec{\nabla}_{\parallel} T, & \delta < r. \end{cases} \tag{15}$$

Substituting Eq. (15) into the continuity equation, while recalling that $\nabla_{\parallel}^2 T = 0$ since the temperature field in our model is linear in x, yields a Laplace equation for the pressure,

$$\nabla_{\parallel}^2 p_0 = 0. \tag{16}$$

The symmetry of the problem suggests a solution of the form $p_0(r, \theta) = R(r) \cos \theta$, which yields a Cauchy-Euler equation for $R(r)$, resulting in $R(r) = ar + \frac{b}{r}$, where a and b are integration constants. We require our solution to be bounded at $r = 0$, yielding

$$p_0(r, \theta) = \begin{cases} a_1 r \cos \theta, & 0 \leqslant r < 1, \\ \left(a_2 r + \frac{b_2}{r} \right) \cos \theta, & 1 < r \leqslant \delta, \\ \left(a_3 r + \frac{b_3}{r} \right) \cos \theta, & \delta \leqslant r, \end{cases} \tag{17}$$
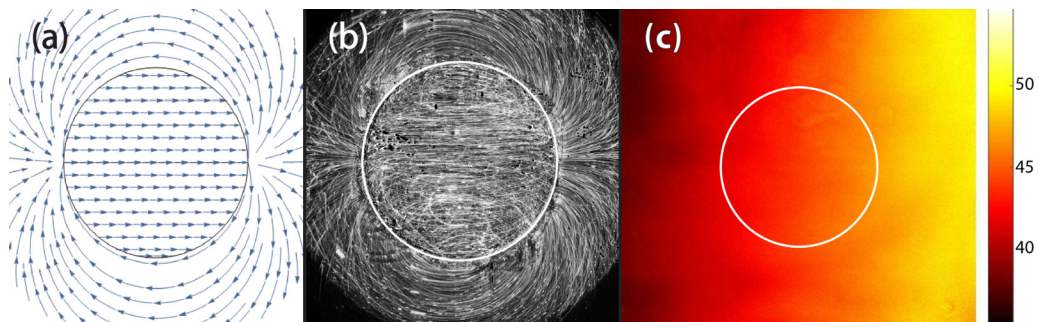
FIG. 2. (a) Theoretically predicted streamlines obtained from Eq. (20). (b) Experimentally measured streamlines for a thermocapillary doublet flow induced in a Hele-Shaw cell by a circular opening of radius $R = 5$ mm subjected to a temperature gradient of 8.8 K/cm. (c) Measurement of the temperature gradient across the Hele-Shaw cell, using a 100 μM rhodamine B solution. For clarity of imaging, the measurement was take in a closed cell without a circular opening. The location of the circular opening corresponding to the dipole experiments is marked with a white circle. The color scale bar corresponds to the temperature in $^\circ$C.

which results in the following expression for the averaged velocity:

$$\langle \vec{u}_0 \rangle = \begin{cases} \left(-\frac{a_1}{3} + \frac{1}{4} + V\right)(\cos\theta, -\sin\theta), & 0 \leqslant r < 1, \\ \left(\left\{\frac{V}{2} - \frac{1}{12}\left[a_2 - \frac{b_2}{r^2}\right]\right\}\cos\theta, -\left\{\frac{V}{2} - \frac{1}{12}\left[a_2 + \frac{b_2}{r^2}\right]\right\}\sin\theta\right), & 1 < r \leqslant \delta, \\ \left(\left\{V - \frac{1}{3}\left[a_3 - \frac{b_3}{r^2}\right]\right\}\cos\theta, -\left\{V - \frac{1}{3}\left[a_3 + \frac{b_3}{r^2}\right]\right\}\sin\theta\right), & \delta \leqslant r. \end{cases} \quad (18)$$

IV. THERMOCAPILLARY DIPOLE

For the limiting case where $\delta \to \infty$ and $V \to 0$, the system corresponds to a Hele-Shaw cell of gap d with a circular opening in its upper plate. We require the velocity to be bounded at infinity, as well as continuity of the pressure and the radial velocity component at $r = 1$, yielding

$$p_0(r, \theta) = \begin{cases} \frac{3}{5} r \cos\theta, & 0 \leqslant r < 1, \\ \frac{3}{5} \frac{1}{r} \cos\theta, & r > 1, \end{cases} \quad (19)$$

$$\langle \vec{u}_0 \rangle = \begin{cases} \frac{1}{20}(\cos\theta, -\sin\theta), & 0 \leqslant r < 1, \\ \frac{1}{20}(\cos\theta, \sin\theta), & r > 1. \end{cases} \quad (20)$$

As shown in Fig. 2(a), the velocity field described by Eq. (20) corresponds to a doublet flow in a Hele-Shaw cell, driven by thermocapillary stresses on the circular free surface, and is consistent with the solution obtained by Rubin *et al.* [15] for nonuniform slip velocity. To implement this configuration, we generated a stable temperature gradient using an 80 mm long aluminum plate, one end of which was heated by a Peltier device while the other end was cooled by a liquid cooler. The temperature was controlled using feedback from two thermocouples placed at each end. On top of the aluminum plate we place a Hele-Shaw chamber consisting of two glass plates separated by a distance $d = 0.4$ mm using a polydimethylsiloxane (PDMS) gasket, with one or several circular openings of radius $R = 5$ mm in the upper plate (see Fig. 1).

To directly measure the temperature within the chamber, we filled it with 100 μM of rhodamine B, a temperature sensitive fluorescent dye, and using a calibration curve (see Appendix) obtained mapping of the temperature. Figure 2(c) presents the resulting temperature distribution, indicating a 4.4 K difference across 5 mm (i.e., 8.8 K/cm). Figure 2(b) presents the experimental streak lines obtained from fluorescent beads used as tracers in the flow, for a uniform temperature gradient of 8.8 K/cm, showing good qualitative agreement with theory. A corresponding video is provided
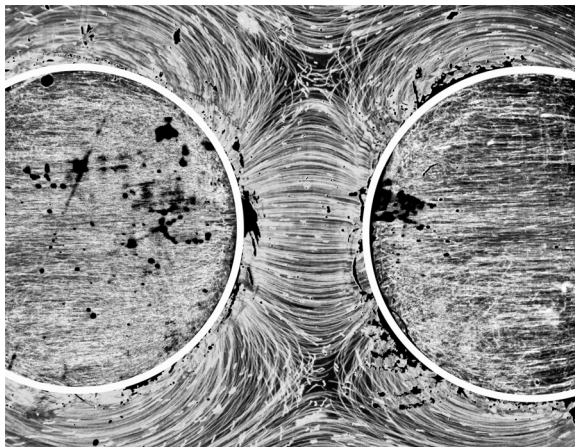
FIG. 3. Experimentally measured streamlines resulting from the superposition of two 5 mm dipoles under a uniform temperature gradient of 8.8 K/cm. The flow between the circular openings is directed from left to right, while above and below the openings the flow is directed from right to left. As expected, two saddle points in the velocity field are formed on the center line between the two openings. Any number of dipoles can be superposed to dictate the flow pattern in the Hele-Shaw chamber.

in the Supplemental Material (SV1) [16]. Figure 3 depicts a superposition of two thermocapillary dipoles, subjected to the same temperature gradient. The flow between the dipoles is directed from left to right, opposite to the induced temperature gradient, while the return flow above and below the openings is directed along the temperature gradient. These opposing flows give rise to two stagnation points in the flow field where the local velocity vanishes. A corresponding video is provided in the Supplemental Material (SV2) [16].

V. THERMOCAPILLARY PUMP

Equation (19) indicates a pressure difference between the two extremes of the circular opening. It is convenient to define a nondimensional, average pressure difference between the two sides of the opening:

$$\langle p \rangle = \frac{1}{\pi} \int_{-\frac{\pi}{2}}^{\frac{\pi}{2}} \Delta p(1, \theta) d\theta = \frac{12}{5\pi}, \tag{21}$$

where $\Delta p(1, \theta) = p(1, \theta) - p(1, \theta + \pi)$. This suggests that if a dipole unit is confined in the direction perpendicular to the temperature gradient, it can act as a thermocapillary motor (TCM), driving liquids through closed microfluidic circuits. In order to test this prediction, we constructed an octagonal confinement with a circular opening 4 mm in diameter, which was connected to a 26 mm long PDMS channel with a rectangular cross section of depth 0.5 mm and width 1 mm, and subjected to a temperature gradient. A schematic description of the TCM experiment is shown in Fig. 4(a). The fluid velocity was measured using particle image velocimetry (PIV) [17].

Figure 4(b) shows the measured maximal velocity in the channel as a function of the temperature difference Δ across the circular opening. A corresponding video is provided in the Supplemental Material (SV5) [16]. This proof of concept experiment demonstrates that a TCM can serve as a pump that, in contrast to pumping mechanisms such as pressure driven or electro-osmotic flow, is capable of driving flows in closed circuits. The velocity is linear with the temperature difference across the channel, and reaches 15 μm/s for a 3 K temperature difference. Since the TCM ultimatley drives the flow via a pressure difference, the modest velocity through the channel can be increased
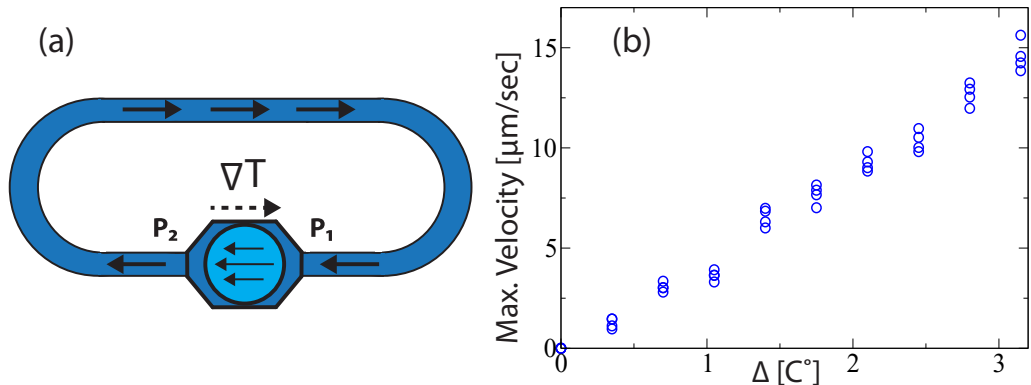
FIG. 4. (a) Schematic of the TCM experiment: a confined dipole configuration is subjected to a temperature gradient $\vec{\nabla}T$, inducing thermocapillary flow across the circular opening. The resulting pressure difference drives the liquid through a closed channel. (b) Experimentally measured maximal velocity as a function of Δ.

by increasing the cross section of the channel, shortening its length or increasing the temperature gradient across the TCM.

VI. THERMOCAPILLARY SURFACE SWIMMER

When δ is finite, the geometry represents an annulus floating on the liquid surface, whose internal opening is subjected to a temperature gradient. We expect such an annulus to reach a steady state velocity V in the direction opposite to that of the temperature gradient. In a frame of reference moving with the annulus we can thus write a boundary condition for the velocity of the liquid at infinity as

$$\lim_{r \to \infty} \langle \vec{u}_0 \rangle \cdot \hat{x} = V. \tag{22}$$

Expanding the left-hand side according to Eq. (27) yields

$$\lim_{r \to \infty} \langle \vec{u}_0 \rangle \cdot \hat{x} = \left[V - \frac{1}{3} \left(a_3 - \frac{b_3}{r^2} \right) \right] \cos^2 \theta + \left[V - \frac{1}{3} \left(a_3 + \frac{b_3}{r^2} \right) \right] \sin^2 \theta = V - \frac{a_3}{3}, \tag{23}$$

and hence

$$a_3 = 0. \tag{24}$$

We demand continuity of the pressure and the radial velocity component at $r = 1$ and $r = \delta$, providing four additional conditions allowing to solve for the remaining coefficients in terms of V which is yet to be resolved:

$$a_1 = -\frac{9 + 18V - \delta^2(5 + 6V)}{-9 + 25\delta^2}, \quad a_2 = -\frac{9 + 18V + 30\delta^2 V}{-9 + 25\delta^2},$$

$$b_2 = \frac{3\delta^2(5 + 16V)}{-9 + 25\delta^2}, \quad b_3 = \frac{6\delta^2(1 - 5(-1 + d^2)V)}{-9 + 25\delta^2}. \tag{25}$$

Since we assume a steady state at which the velocity of the swimmer is constant, the net force on it must be zero. The two forces acting on the swimmer are the surface tension and the viscous drag. The integral of surface tension over the inner perimeter of the annulus vanishes (similar to an elastic sheet stretched across a circular opening), and since we assume the temperature outside the annulus is uniform, the integral of surface tension there vanishes as well. Thus, the viscous drag term must
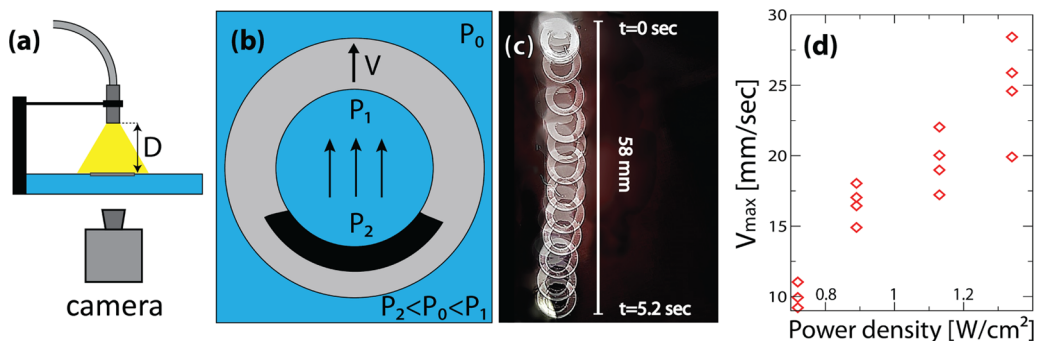
FIG. 5. (a) Side-view schematic illustration of the surface swimmer experimental setup. The illumination source is located at a distance D from the swimmer, controlling the power density on the swimmer. (b) Top-view schematic of the surface swimmer. The projected light heats the black stripe on the inner side of the annulus, inducing a temperature gradient across the opening. (c) A set of time-lapse overlaid images showing the swimmer's propagation under uniform illumination. (d) Experimental measurements of the maximal velocity of the swimmer as a function of power density, actuated in tap water.

also vanish, yielding

$$0 = \int_{R_1}^{R_2} \int_0^{2\pi} \mu \frac{\partial \tilde{u}_0}{\partial \tilde{z}} \Bigg|_{z=1} \cdot \hat{x} \, \tilde{r} \, d\tilde{r} = \sigma_T \Delta R_1 (\delta^2 - 1) \left(\frac{a_2}{2} - V \right), \tag{26}$$

hence

$$V = \frac{a_2}{2} = \frac{9}{80\delta^2}, \quad \delta > 1, \tag{27}$$

and in dimensional form

$$\tilde{V} = V \frac{d\sigma_T \Delta}{R_1 \mu} = \frac{9 d \sigma_T \Delta R_1}{20 R_2^2 \mu}. \tag{28}$$

As expected, the velocity of propulsion tends to zero as $\delta \to \infty$.

This result, which strictly holds only for the case of a shallow liquid film, can be heuristically extended for a swimmer on the surface of an infinite water bath by taking d to be the velocity decay distance. One such estimate for the decay distance in thermocapillary driven flows is given by Napolitano [18] to be $d = \sqrt{\frac{R\nu}{U}}$, where R is the length of the free surface and U is the characteristic velocity. For our problem

$$U = \frac{d\sigma_T \Delta}{R\mu} \implies d = \left(\frac{R^2 \mu^2}{\sigma_T \rho \Delta} \right)^{\frac{1}{3}} \implies \epsilon \approx 0.1 \Delta^{-1/3}, \tag{29}$$

consistent with the assumptions of the model. If we take the liquid to be water, using $\delta = \frac{5}{4}$ as in our experiments, the resulting predicted velocity of the surface swimmer is $\tilde{V} \approx 20$ mm/s for a temperature difference of $\Delta = 4$ °C.

To implement a thermocapillary surface swimmer, we used an annulus made of white polystyrene, with thickness ≈ 240 μm, an outer radius $R_2 = 8$ mm, and inner radii between $R_1 = 3$ and 5 mm. We painted a black stripe on its inner side [see Fig. 5(b)], and used a halogen light source to illuminate the system in order to create a temperature gradient across the inner opening. We recorded the motion of the swimmer by video, and measured its velocity as a function of the projected power density, controlled by varying the distance between the light source and the liquid's surface. Figure 5(c) presents an overlaid set of images showing the location of the surface swimmer as a function of time, in response to sudden exposure to a light source concentric with its location
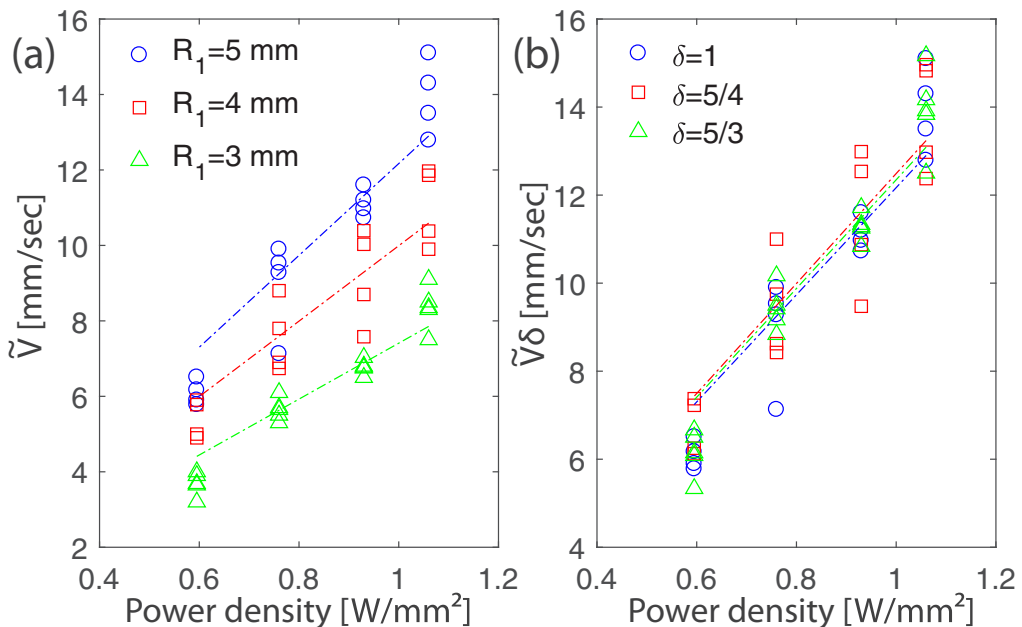
FIG. 6. (a) The dimensional average velocity of the surface swimmer as a function of the power density of the light source. Circles, squares and asterisks correspond to $R_1 = 5, 4$, and 3, respectively. (b) The dimensional average velocity of the surface swimmer normalized by δ. Dashed lines correspond to a best fit of each data set to a linear curve forced through the origin. The overlap of the curves in the normalized case shows good agreement with the scaling given by Eq. (28).

at $t = 0$. The light absorbed by the black stripe induces a temperature gradient, pushing the surface swimmer in the direction opposite to the location of the stripe. In all experiments we observed an initial acceleration of the swimmer, followed by a decay of its velocity as it leaves the illuminated region. This is shown in supplemental video SV3, whereas supplemental video SV4 shows a case where we follow the swimmer with the light source, resulting in its continuous motion [16]. Figure 5(d) depicts the measured maximal velocity of the surface swimmer, for a given power density of the projected light. We measured velocities of up to 28 mm/s, a significant value in the context of microflows. We note that these experiments were conducted using plain tap water in order to demonstrate the robustness of the system. These results are in good agreement with the estimated value of $U_s \approx 20$ mm/s, obtained from Eq. (28), using our experimental parameters and for a typical value of $\Delta = 4\,^\circ$C. Figure 6(a) shows the velocity of different swimmers having a fixed outer radius and different inner radii, as a function of light intensity. To allow proper comparison between the cases, these experiments were conducted using controlled liquid properties [in contrast to the tap water demonstration in Fig. 5(c)] using deionized water with a 100 mM salt concentration. Figure 6(b) shows the measured velocities normalized by δ. In both figures, the dashed lines correspond to linear best fits to each data set. The resulting slope values for the normalized velocities are 12.3, 12.5, and 12.2 for the 3, 4, and 5 mm swimmers, respectively; i.e., the three data sets can be described by a single linear curve, in support of the scaling scaling given by Eq. (28).

VII. SUMMARY AND DISCUSSION

In this paper we demonstrated that thermocapillary flow across a circular opening in a Hele-Shaw type configuration induces a dipole flow inside the Hele-Shaw cell and that such flows could be superposed to obtained two-dimensional flow patterns. A potential extension of this work is the

design of flow patterns by distributions of dipoles of different strengths across the flow chambers. This could be achieved using different cavity radii, all subjected to a uniform temperature gradient, or alternatively by localized heating (e.g., by electrodes or illumination) which would allow one to control not only the magnitude but also the direction of each dipole. It would also be of interest to explore mass transport in such systems; since the dipole flow has a zero net mass flux, multiple dipoles could be used, for example, to accelerate the mixing between different fluidic chambers in microfluidic applications. We showed that a confined dipole can act as a thermocapillary motor for driving liquids. This mechanism of pumping may be particularly useful in microfluidic applications as it allows driving flow in a closed circuit. This in contrast to other standard mechanisms, such as pressure driven flow or electro-osmotic flow, which are inherently directional. The TCM is modular in the sense that it can be positioned in-line in any microfluidic channel. It would thus be of interest to study the effects of various combinations of TCM units (in linear or parallel configurations) on the resulting flow rate.

We have demonstrated that a mobile dipole in the form of an annulus can be turned into a thermocapillary surface swimmer, reaching velocities on the order of 20 mm/s. Importantly, unlike laser-induced motion requiring accurate positioning and tracking, the swimmers we present can be actuated using simple uniform illumination from above at moderate intensities of order 1 W/cm^2. Furthermore, the swimmers do not require a specialized liquid and operate robustly in plain tap water.

While a large body of work exists on a variety of physical mechanisms for swimmers that are suspended in the bulk of the liquid [19], the unique physics of interfacial phenomena provides different and interesting mechanisms for surface-based propulsion of swimmers. It is interesting to compare the thermocapillary surface swimmer to other methods of Marangoni propulsion, such as the thin rigid circular disk studied theoretically by Lauga and Davis [20]. There, the disk's propulsion was driven by an external surface tension gradient caused by the release of an insoluble surfactant from part of the disk's perimeter. In contrast, the thermocapillary swimmer is driven by an internal surface tension gradient, with minimal effect on the surrounding environment. In addition, the thermocapillary swimmer's velocity is directed oppositely to the temperature gradient, and is aligned with the surface tension gradient, suggesting that a combination of an external and an internal surface tension gradients should result in an increase of the propulsion velocity. Thermocapillary surface swimmers could potentially be produced on the microscale and in large quantities, and it may be or interest to explore their use as a means for fluidic photoactivation. This would, however, require further understanding of the viability of such propulsion mechanisms with the decrease in the dimensions of the system.

APPENDIX: MATERIALS AND METHODS

1. Temperature gradient system

In order to create a stable temperature gradient we used an 80 mm $\times$ 25 mm $\times$ 3 mm aluminum plate, one end of which was heated by a Peltier device while the other end was cooled by a liquid cooler (CORSAIR H110i liquid CPU cooler); see Fig. 7. We measured the temperature difference using two thermocouples placed on each end of the aluminum plate, connected to a temperature controller device (KR1, Ascon Tecnologic, Italy).

2. Imaging conditions and temperature calibration curve

For flow visualization, we used 2 μm fluorescent beads (Fluoro-Max, Thermo Scientific, Fremont, CA, USA) premixed in deionized water. The fluroescence in the chamber was imaged
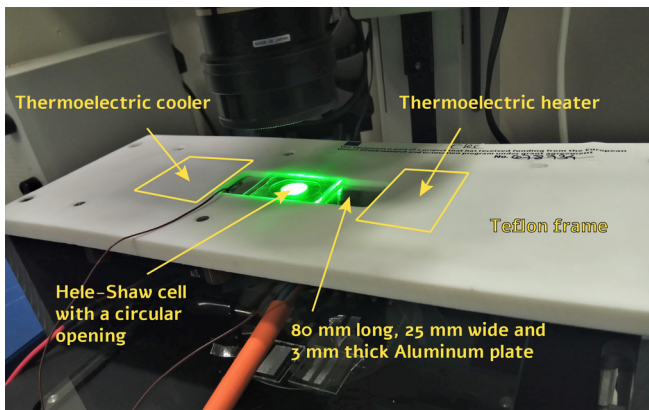
FIG. 7. Photograph of the experimental setup for the thermocapillary dipole experiment. The setup consists of an 80 mm aluminum plate, one end of which was heated by a Peltier device while the other end was cooled by a liquid cooler. The temperature was controlled using feedback from two thermocouples placed at each end. On top of the aluminum plate we placed a Hele-Shaw chamber consisting of two glass plates separated by distance $d = 0.4$ mm using a PDMS gasket, with one or several circular openings of radius $R = 5$ mm in the upper plate.

using an epifluorescent microscope (AZ100, Nikon, Tokyo, Japan) equipped with a metal halide light source (Intensilight, Nikon, Japan) and a Chroma 49011 filter cube (545/25 nm excitation, 605/70 nm emission and 565 nm dichroic mirror). We used an AZ-Plan Apo $1\times$ objective (NA 0.1, WD 35 mm) in all the experiments. Images were captured using a 12 bit, 4.2 megapixel, sCMOS camera (Zyla 4.2 sCMOS, Andor, Belfast, Ireland). We triggered the camera at intervals of 1 s with
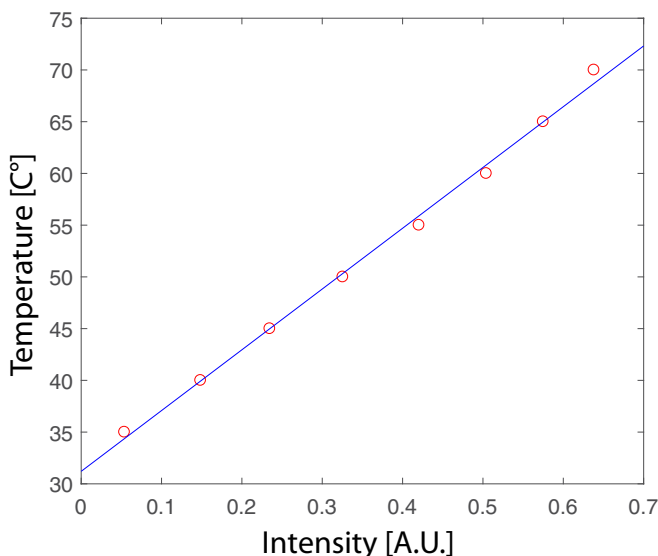
FIG. 8. Calibration curve relating temperature to rhodamine B intensity (in arbitrary units). We placed the fluidic chamber on top of an indium-tin-oxide (ITO) heating device providing a controlled uniform temperature. We changed the temperature at fixed intervals of $5°$, and for each one imaged the dye intensity in the chamber. The images were flat-field corrected according to the intensity at room temperature, and then averaged over a fixed area. We fit the data to a linear curve, and use it to measure the temperature gradient in the dipole experiments.

an exposure time of 1 s. We controlled the camera using NIS ELEMENTS software (v.4.11, Nikon) and processed the images with MATLAB (R2011b, Mathworks, Natick, MA). For the TCM experiment, the fluid velocity was measured using PIVLAB: Time Resolved Digital Particle Image Velocimetry Tool for MATLAB. We measured the temperature gradient across the Hele-Shaw chamber using a 100 μM solution of rhodamine B. The intensity of rhodamine B was translated into temperature using a calibration curve which is given in Fig. 8.

3. Thermocapillary surface swimmer

We used a fiber bundle coupled halogen light source (OSL1-EC, Thorlabs, Newton, New Jersey, USA) to illuminate the system in order to create a temperature gradient across the inner opening. The swimmer was placed in a transparent Petri dish, and we recorded the motion of the swimmer by video using a consumer-grade camera located on top of a gridded surface. The velocity was extracted manually by measuring the displacement of the surface swimmer between frames. The power density was controlled by varying the distance between the light source and the surface of the liquid, and measured for a given distance by an optical power meter (PM100D, Thorlabs, Newton, New Jersey, USA).

[1] A. Karbalaei, R. Kumar, and H. J. Cho, Thermocapillarity in microfluidics—A review, Micromachines **7**, 13 (2016).

[2] T. S. Sammarco and M. A. Burns, Thermocapillary pumping of discrete drops in microfabricated analysis devices, AIChE J. **45**, 350 (1999).

[3] C. N. Baroud, J.-P. Delville, F. Gallaire, and R. Wunenburger, Thermocapillary valve for droplet production and sorting, Phys. Rev. E **75**, 046302 (2007).

[4] A. D. Stroock, R. F. Ismagilov, H. A. Stone, and G. M. Whitesides, Fluidic ratchet based on Marangoni-Bénard convection, Langmuir **19**, 4358 (2003).

[5] M. Dietzel and S. M. Troian, Thermocapillary patterning of nanoscale polymer films, MRS Proc. **1179**, 1179-BB08-02 (2009).

[6] N. Garnier, R. O. Grigoriev, and M. F. Schatz, Optical Manipulation of Microscale Fluid Flow, Phys. Rev. Lett. **91**, 054501 (2003).

[7] C. Maggi, F. Saglimbeni, M. Dipalo, F. De Angelis, and R. Di Leonardo, Micromotors with asymmetric shape that efficiently convert light into work by thermocapillary effects, Nat. Commun. **6**, 7855 (2015).

[8] D. Okawa, S. J. Pastine, A. Zettl, and J. M. J. Fréchet, Surface tension mediated conversion of light to work, J. Am. Chem. Soc. **131**, 5396 (2009).

[9] A. Girot, N. Danné, A. Würger, T. Bickel, F. Ren, J. C. Loudet, and B. Pouligny, Motion of optically heated spheres at the water-air interface, Langmuir **32**, 2687 (2016).

[10] V. Frumkin, W. Mao, A. Alexeev, and A. Oron, Creating localized-droplet train by traveling thermal waves, Phys. Fluids **26**, 082108 (2014).

[11] V. Frumkin and A. Oron, Liquid film flow along a substrate with an asymmetric topography sustained by the thermocapillary effect, Phys. Fluids **28**, 082107 (2016).

[12] W. Boos and A. Thess, Thermocapillary flow in a Hele-Shaw cell, J. Fluid Mech. **352**, 305 (1997).

[13] T. Baier, C. Steffes, and S. Hardt, Thermocapillary flow on superhydrophobic surfaces, Phys. Rev. E **82**, 037301 (2010).

[14] E. Yariv, Thermocapillary flow between longitudinally grooved superhydrophobic surfaces, J. Fluid Mech. **855**, 574 (2018).

[15] S. Rubin, A. Tulchinsky, A. D. Gat, and M. Bercovici, Elastic deformations driven by non-uniform lubrication flows, J. Fluid Mech. **812**, 841 (2017).

[16] See Supplemental Material at http://link.aps.org/supplemental/10.1103/PhysRevFluids.4.074002 for videos showing the flow due to a single thermocapillary dipole (SV1), the flow due to superposition

of dipoles (SV2), the motion of a thermocapillary surface swimmer under a stationary light source (SV3) and a moving light source (SV4), as well as the pumping action of the thermocapillary motor (SV5).

[17] W. Thielicke and E. Stamhuis, PIVlab—Towards user-friendly, affordable and accurate particle image velocimetry in MATLAB, J. Open Res. Software **2**, 30 (2014).

[18] L. Napolitano, Marangoni boundary layers, in *Proceedings of the Third European Symposium on Material Sciences in Space* (ESA, Paris, 1979), pp. 349–358.

[19] J. Elgeti, R. G. Winkler, and G. Gompper, Physics of microswimmers—Single particle motion and collective behavior: A review, Rep. Prog. Phys. **78**, 056601 (2015).

[20] E. Lauga and A. M. J. Davis, Viscous Marangoni propulsion, J. Fluid Mech. **705**, 120 (2012).